nature physics

SUPPLEMENTARY INFORMATION

https://doi.org/10.1038/s41567-019-0594-5

In the format provided by the authors and unedited.

Field-tunable quantum disordered ground state in the triangular-lattice antiferromagnet $NaYbO_2$

Mitchell M. Bordelon[1], Eric Kenney[2], Chunxiao Liu[3], Tom Hogan[4], Lorenzo Posthuma[1], Marzieh Kavand[5], Yuanqi Lyu[5], Mark Sherwin[5], N. P. Butch[6], Craig Brown[6,7], M. J. Graf[2], Leon Balents[8] and Stephen D. Wilson[1]*

[1]Materials Department, University of California, Santa Barbara, Santa Barbara, CA, USA. [2]Department of Physics, Boston College, Chestnut Hill, MA, USA. [3]Department of Physics, University of California, Santa Barbara, Santa Barbara, CA, USA. [4]Quantum Design, Inc., San Diego, CA, USA. [5]Department of Physics and Center for Terahertz Science and Technology, University of California, Santa Barbara, Santa Barbara, CA, USA. [6]NIST Center for Neutron Research, National Institute of Standards and Technology, Gaithersburg, MD, USA. [7]Department of Chemical and Biomolecular Engineering, University of Delaware, Newark, DE, USA. [8]Kavli Institute for Theoretical Physics, University of California, Santa Barbara, Santa Barbara, CA, USA.
*e-mail: stephendwilson@ucsb.edu

Supplemental Material: Field-tunable quantum disordered ground state in the triangular lattice antiferromagnet $NaYbO_2$

Mitchell M. Bordelon, Eric Kenney, Chunxiao Liu, Tom Hogan, Lorenzo Posthuma, Marzieh Kavand, Yuanqi Lyu, Mark Sherwin, Craig Brown, N. P. Butch, M. J. Graf, Leon Balents, Stephen D. Wilson

June 12, 2019

1 Symmetry and Exchange Interactions

In this Supplemental section, we discuss the symmetries and show that the symmetry-allowed exchange interactions on the nearest-neighbor in-plane and inter-layer bonds have the form given in the main text. In $NaYbO_2$, the magnetic Yb atoms live on the sites of 2d triangular lattices with "ABC" stacking in the vertical direction. This is a rhombohedral lattice. Specifically, the system has space group 166, $R\bar{3}m$. We assume that the there is an effective spin-1/2 operator transforming like a pseudo-vector on each Yb site. The exchange interactions on a bond are constrained by the subgroup of the full space group which preserves that bond, i.e. which leaves the center of the bond unchanged. We discuss the intra-layer and inter-layer bonds in turn below.

In this and the following Supplemental section, it will be useful to establish notation. In conventional rhombohedral coordinates, we specify positions using dimensionless coordinates so that

$$\boldsymbol{r}_{mnl} = m\boldsymbol{a}_1 + n\boldsymbol{a}_2 + l\boldsymbol{c}, \tag{1}$$

with vectors

$$\boldsymbol{a}_1 = a(1,0,0), \tag{2}$$

$$\boldsymbol{a}_2 = a(-\frac{1}{2}, \frac{\sqrt{3}}{2}, 0), \tag{3}$$

$$\boldsymbol{c} = c(0,0,1). \tag{4}$$

Note that $\boldsymbol{c}$ is not the primitive translation but a conventional one. The primitive translation is $(2\boldsymbol{a}_1 + \boldsymbol{a}_2 + \boldsymbol{c})/3$. This connects a layer at $l = 0$ to $l = 1/3$.

1.1 NN in-plane bonds

All the in-plane bonds are equivalent by rotations and translations. So we can deduce the exchange on all of them by considering one. Specifically, we consider one whose center is at coordinates $(1/2, 0, 0)$. This is the middle of a bond along the x axis in cartesian coordinates. This point is the 9e Wyckoff position, with site symmetry group 2/m. The point group is generated by 2 $\mathbb{Z}_2$ operations, which we can take as: (1) inversion through the bond center and (2) a C_2 rotation about the axis along the bond. Composing these two gives a third (not independent) element, a mirror reflection through the plane normal to the bond. Using these operations, we learn from inversion that there is no DM coupling. Then applying the C_2 operation, for a bond along x, the sites are *not* interchanged but $S_i^y \to -S_i^y$ and $S_i^z \to -S_i^z$. This means the general exchange matrix for a bond connecting the two sites along this direction is

$$J_{NN,\boldsymbol{x}} = \begin{pmatrix} J_1 & 0 & 0 \\ 0 & J_2 & J_4 \\ 0 & J_4 & J_3 \end{pmatrix}. \tag{5}$$

Now we obtain the exchange for an arbitrary pair of in-plane NN spins by rotation. The general form is

$$H_{2d} = \sum_{\langle ij \rangle} \left\{ J_{xy} \left(S_i^x S_j^x + S_i^y S_j^y \right) + J_z S_i^z S_j^z + J_c \left(\hat{\boldsymbol{e}}_{ij} \cdot \boldsymbol{S}_i \right) \left(\hat{\boldsymbol{e}}_{ij} \cdot \boldsymbol{S}_j \right) + J_{cz} \left[\left(\hat{\boldsymbol{z}} \cdot \hat{\boldsymbol{e}}_{ij} \times \boldsymbol{S}_i \right) S_j^z + \left(\hat{\boldsymbol{z}} \cdot \hat{\boldsymbol{e}}_{ij} \times \boldsymbol{S}_j \right) S_i^z \right] \right\}. \quad (6)$$

Here $\hat{\boldsymbol{e}}_{ij}$ is the unit vector along the bond direction, and lies in the xy plane. The J_{xy} and J_z terms comprise an XXZ model, J_c is a "compass" interaction, and J_{cz} combines in-plane and out-of-plane components with some compass-like anisotropy. Specifically it couples the component of spin normal to the bond but within the plane to the out of plane component.

This form is equivalent to that written down in Ref.[3]. The relation between the form used here and the one in Ref.[3] can be found in Ref.[1].

1.2 Out of plane bonds

The out of plane bonds are not vertical, but connect each spin in a layer to three spins above and three spins below. As above, we consider the point symmetry group of a mid-point of such a bond. An example is the point $(1/3, 1/6, 1/6)$ in lattice coordinates. This is the mid-point of a bond whose projection into the xy plane is at a 30 degree angle to the x axis, i.e which bisects a triangle of the triangular plane. This is the 9d Wyckoff position, which *also* has site symmetry 2/m. The group is the same as for the in-plane bond, but the symmetries are slightly different. The two generators in this case can be considered as: (1) inversion and (2) a C_2 rotation which is about an axis which bisects the bond and is parallel to the xy plane. The two composed together give the third non-trivial operation in the point group which is a mirror plane which contains the bond and is normal to the xy plane. The difference from the previous case is the orientation of the C_2 axis or the plane of the mirror. The result is that the effective exchange interaction has a very slightly different form from Eq. (6)

$$H' = \sum_{\langle\langle ij \rangle\rangle} \left\{ J'_{xy} \left(S_i^x S_j^x + S_i^y S_j^y \right) + J'_z S_i^z S_j^z + J'_c \left(\hat{\boldsymbol{f}}_{ij} \cdot \boldsymbol{S}_i \right) \left(\hat{\boldsymbol{f}}_{ij} \cdot \boldsymbol{S}_j \right) + J'_{cz} \left[\left(\hat{\boldsymbol{f}}_{ij} \cdot \boldsymbol{S}_i \right) S_j^z + \left(\hat{\boldsymbol{f}}_{ij} \cdot \boldsymbol{S}_j \right) S_i^z \right] \right\}, \quad (7)$$

where i and j are closest sites in neighboring layers, and $\hat{\boldsymbol{f}}_{ij}$ is a unit vector along the *projection* of the bond direction into the xy plane, and so also lies in this plane. The vectors $\hat{\boldsymbol{e}}_{ij}$ appearing in Eq. (6) are oriented along the triangular axes, while the $\hat{\boldsymbol{f}}_{ij}$ vectors bisect these directions. The other difference from Eq. (6) is that in Eq. (7), the final term has no cross product. That is a result of the different orientation of rotation axis/mirror plane in this second situation.

This completes the symmetry analysis of interactions. Eq. (6) and Eq. (7) are reproduced in the main text.

2 Classical Phases and Frustration

In this Supplemental section, we discuss aspects of the classical ground states of the model Hamiltonian given in Eqs. (68), and to what extent frustration arises therein.

2.1 Two dimensional case

Since we expect that the interlayer interactions are small compared to the intralayer ones in practice, we begin by discussing what is known for the two dimensional model, with all interlayer interactions turned off. This Hamiltonian has already been extensively studied. It is a simple extension of the "compass" model on the triangular lattice, which had been considered long ago. Collecting results from many papers[1, 9, 4, 2], there are three types of classical ground states which emerge for nearly all parameters in the antiferromagnetic regime: a three-sublattice 120° planar state, and two collinear stripe states, which differ from one another only in the direction of their spin polarization.

2.1.1 Classical three-sublattice states

First we consider the three-sublattice 120° states. It is helpful to rewrite the Hamiltonian a bit more explicitly. For a single layer, we can write

$$H_{2d} = \sum_i \sum_{\mu=1,2,3} \Big\{ J_{xy} \left(S_i^x S_{i+\mu}^x + S_i^y S_{i+\mu}^y \right) + J_z S_i^z S_{i+\mu}^z + J_c \left(\boldsymbol{a}_\mu \cdot \boldsymbol{S}_i \right) \left(\boldsymbol{a}_\mu \cdot \boldsymbol{S}_{i+\mu} \right) + J_{cz} \left[\left(\hat{\boldsymbol{z}} \cdot \boldsymbol{a}_\mu \times \boldsymbol{S}_i \right) S_{i+\mu}^z + \left(\hat{\boldsymbol{z}} \cdot \boldsymbol{a}_\mu \times \boldsymbol{S}_{i+\mu} \right) S_i^z \right] \Big\}. \tag{8}$$

Here we took $\boldsymbol{a}_3 = -\boldsymbol{a}_1 - \boldsymbol{a}_2$.

Now consider a general three-sublattice state, in which for site $i = (m,n)$ in lattice coordinates

$$\boldsymbol{S}_{m,n} = S \boldsymbol{n}_{\mathrm{Mod}[-m-n,3]}, \tag{9}$$

with three classical fixed length vectors $\boldsymbol{n}_s$ with $s = 0,1,2$ labeling the three sublattices. For such a state, the energy becomes

$$3E_{2d}/(NS^2) = \sum_{s=0,1,2} \Big\{ 3J_{xy} \left(n_s^x n_{s-1}^x + n_s^y n_{s-1}^y \right) + 3J_z n_s^z n_{s-1}^z + J_c \sum_\mu \left(\boldsymbol{a}_\mu \cdot \boldsymbol{n}_s \right) \left(\boldsymbol{a}_\mu \cdot \boldsymbol{n}_{s-1} \right) + J_{cz} \sum_\mu \left[\left(\hat{\boldsymbol{z}} \cdot \boldsymbol{a}_\mu \times \boldsymbol{n}_s \right) n_{s-1}^z + n_s^z \left(\hat{\boldsymbol{z}} \cdot \boldsymbol{a}_\mu \times \boldsymbol{n}_{s-1} \right) \right] \Big\} \tag{10}$$

Here we have written sublattice s modulo 3. The sum over μ can be carried out explicitly. The last term vanishes because $\sum_\mu \boldsymbol{a}_\mu = 0$. In the second last term, we use $\sum_\mu \boldsymbol{a}_\mu \boldsymbol{a}_\mu^T = (3/2)\mathrm{diag}(1,1,0)$. We obtain

$$3E_{2d}/(NS^2) = \sum_{s=0,1,2} \left[3 \left(J_{xy} + \frac{J_c}{2} \right) \left(n_s^x n_{s-1}^x + n_s^y n_{s-1}^y \right) + 3J_z n_s^z n_{s-1}^z \right]. \tag{11}$$

We observe the remarkable emergence of U(1) symmetry of the classical energy, despite the anisotropy of the Hamiltonian. This is a well-known accidental degeneracy which occurs for many compass models.[5] Note that vanishing effect of in-plane anisotropy and the complete absence of any effect from J_{cz} is general for any three-sublattice state with this unit cell, whether the spins be collinear, coplanar, or otherwise. It would also hold within any Curie-Weiss mean field treatment which would allow for variable magnitude of the local spin expectation values. The three-sublattice ordered state occurs when the first term above dominates, and the spins consequently orient in the plane with three different sublattice orientations at 120° angles to one another. Frustration is evident in this ordered pattern by the fact that the classical energy is independent of the overall angle of the spins within the XY plane, which is not related to any symmetry of the model.

Note that when J_z is sufficiently large, the lowest energy configurations of the three sublattice state become Ising like, with spins oriented normal to the plane. However, in this regime the global ground states are actually not of the three-sublattice form, but rather the stripe states we consider next.

2.1.2 Classical stripe phases

If the compass interaction J_c dominates, it is natural to select spins to be aligned or anti-aligned along appropriate neighbors. For example, if we take $J_c < 0$, the compass coupling for an $\boldsymbol{a}_1 = \hat{\boldsymbol{x}}$ bond would favor spins oriented along the x direction forming ferromagnetic chains along this axis. Let us just assume to start a two-sublattice structure, so that

$$\boldsymbol{S}_{m,n} = S \boldsymbol{n}_{\mathrm{Mod}[n,2]}, \tag{12}$$

i.e. with ferromagnetic chains along x. Inserting this into Eq. (8), we obtain an energy

$$\frac{2E}{NS^2} = J(2 + 4\boldsymbol{n}_0 \cdot \boldsymbol{n}_1) + J_z \left(4 n_0^z n_1^z + (n_0^z)^2 + (n_1^z)^2 \right) + J_c \left((n_0^x)^2 + (n_1^x)^2 + n_0^x n_1^x + 3 n_0^y n_1^y \right) + J_{cz} XX, \tag{13}$$

where we did not write the expression for the J_{cz} term, because we are going to focus on in-plane order (favored for negative J_z). Assuming in-plane order, i.e. $n_a^z = 0$, the energy is minimized for spins aligned along the y direction:

$$\boldsymbol{n}_0 = -\boldsymbol{n}_1 = \pm\hat{\boldsymbol{y}}, \qquad \frac{2E}{NS^2} = -2J_{xy} - 3J_c. \tag{14}$$

The above equations describe two solutions for stripe states, which are translations and time-reversals of one another. There are another four such states, obtain by C_3 rotations of these two, where the ferromagnetic stripes lie along other axes. Note this 6-fold degeneracy of the stripe states is *not* accidental, but symmetry mandated. There is no accidental degeneracy within the stripe ground states, and hence we may regard them as less frustrated than the 120° three sublattice states.

One can compare the energy for these states to that for the 120° states, by examining Eq. (11). For the 3 sublattice states, one has $\boldsymbol{n}_s \cdot \boldsymbol{n}_{s-1} = -1/2$. One obtains the energy per spin in the two cases as

$$E_{120}/(NS^2) = -\frac{3}{2}J_{xy} - \frac{3}{4}J_c, \qquad E_{stripe}/(NS^2) = -J_{xy} - \frac{3}{2}J_c. \tag{15}$$

Clearly the 120 degree state is better for small J_c and the stripe state is better for larger J_c. One finds the stripe is favorable once $J_c > 2/3J_{xy}$.

2.1.3 Adding magnetic field

Now we study the classical ground state of the two dimensional model (6) in presence of a magnetic field. The field dependence enters the Hamiltonian through the Zeeman term

$$H_{2d,B} = H_{2d} - \mu_B \sum_i \left[g_{xy}(B^x S_i^x + B^y S_i^y) + g_z B^z S_i^z \right]. \tag{16}$$

We will assume a general three-sublattice state as in Eq. (9). Under this assumption the classical energy becomes

$$3E_{2d,B}/(NS^2) = 3E_{2d}/(NS^2) - (\mu_B/S) \sum_{s=0,1,2} \left[g_{xy}(B^x n_s^x + B^y n_s^y) + g_z B^z n_s^z \right]. \tag{17}$$

For simplicity, we define dimensionless parameters

$$r \equiv \frac{J_{xy} + J_c/2}{J_z}, \qquad m_x \equiv \frac{\mu_B g_{xy} B^x}{3S(J_{xy} + J_c/2)}, \qquad m_y \equiv \frac{\mu_B g_{xy} B^y}{3S(J_{xy} + J_c/2)}, \quad \text{and} \quad m_z \equiv \frac{\mu_B g_z B^z}{3SJ_z}. \tag{18}$$

The classical phase diagram for a perpendicular field (i.e. $m_x = m_y = 0$) is easily found (see e.g. Ref. [8]). As the field develops an in-plane component, the classical spin vectors rotates continuously. In the easy-plane anisotropy region ($r > 1$) of the (r, m_x, m_y, m_z) phase space, the phase diagram can be analytically obtained:

$$\begin{cases} r > 1 \text{ and } \frac{m_x^2}{9} + \frac{m_y^2}{9} + \frac{m_z^2}{(r+2)^2} \geq 1: & \text{“paramagnetic” phase;} \\ r > 1 \text{ and } \frac{m_x^2}{9} + \frac{m_y^2}{9} + \frac{m_z^2}{(r+2)^2} < 1: & \text{“canted” phase.} \end{cases} \tag{19}$$

The “paramagnetic” phase has unique classical ground state in which spins are maximally aligned to minimize the classical energy $E_{2d,B}$. Note that this is not a real paramagnet in the sense that the aligned spin orientation is not necessarily the same as the field orientation (hence the quote). In the “canted” phase, the classical ground states are accidentally degenerate and form a one-dimensional manifold, subject to the following constraints

$$n_0^z = n_1^z = n_2^z = \frac{3m_z}{r+2}, \qquad n_0^x + n_1^x + n_2^x = m_x, \quad \text{and} \quad n_0^y + n_1^y + n_2^y = m_y. \tag{20}$$

In the easy-axis anisotropy region ($0 < r < 1$) the complete phase diagram is complicated. Nevertheless we are able to separate the “paramagnetic” phase from the others:

$$\begin{cases} 0 < r < 1 \text{ and } \frac{m_x^2}{(1/r+2)^2} + \frac{m_y^2}{(1/r+2)^2} + \frac{m_z^2}{(r+2)^2} \geq 1: & \text{“paramagnetic” phase;} \\ 0 < r < 1 \text{ and } \frac{m_x^2}{(1/r+2)^2} + \frac{m_y^2}{(1/r+2)^2} + \frac{m_z^2}{(r+2)^2} < 1: & \text{coplanar phases.} \end{cases} \tag{21}$$

2.2 Inter-layer effects

Next we consider the effect of couplings between the layers. We regard the inter-layer couplings always as small compared to the intra-layer ones. Thus to a first approximation, we ask how the interlayer Hamiltonian, H', behaves when *projected* into the space of states whose order or correlations is set by the 2d interactions.

2.2.1 Three-sublattice regime

If the 2d system is in the regime with three-sublattice correlations, we should consider the energy of an arbitrary state with the three-sublattice structure *in each layer*, and find the energy due to interlayer couplings. We further assume that the system is periodic under translation by three layers. There will then be 9 sublattices, labeled by a sublattice index $s = 0, \ldots, 9$. We can define this by the condition

$$\boldsymbol{S}_i = S\boldsymbol{n}_s, \qquad \boldsymbol{r}_i = m\boldsymbol{a}_1 + n\boldsymbol{a}_2 + \frac{l}{3}(2\boldsymbol{a}_1 + \boldsymbol{a}_2 + \boldsymbol{c}), \qquad s = 3\mathrm{Mod}[l,3] + \mathrm{Mod}[-m-n,3]. \tag{22}$$

Now we can express the inter-layer energy in terms of the 9 sublattice magnetizations $\boldsymbol{n}_s$:

$$\begin{aligned} 9E_{il}/(NS^2) = \sum_{l=0}^{2}\sum_{p=0}^{2}\sum_{q=0}^{2} \Big\{ & J'_{xy}\left(n^x_{s(l,p)}n^x_{s'(l,p,q)} + n^y_{s(l,p)}n^y_{s'(l,p,q)}\right) + J'_z n^z_s n^z_{s'} + J'_c\left(\boldsymbol{f}_q\cdot\boldsymbol{n}_s\right)\left(\boldsymbol{f}_q\cdot\boldsymbol{n}_{s'}\right) \\ & + J'_{cz}\left[\left(\boldsymbol{f}_q\cdot\boldsymbol{n}_s\right)n^z_{s'} + n^z_s\left(\boldsymbol{f}_q\cdot\boldsymbol{n}_{s'}\right)\right]\Big\}, \end{aligned} \tag{23}$$

where

$$s(l,p) = 3l + p, \qquad s'(l,p,q) = 3\mathrm{Mod}[l+1,3] + \mathrm{Mod}[p+q,3], \tag{24}$$

and

$$\boldsymbol{f}_q = \begin{pmatrix} \cos\left(\frac{\pi}{6} + \frac{2\pi q}{3}\right) \\ \sin\left(\frac{\pi}{6} + \frac{2\pi q}{3}\right) \\ 0 \end{pmatrix}. \tag{25}$$

The first two terms can be readily rewritten to simplify the energy to

$$\begin{aligned} 9E_{il}/(NS^2) = \sum_{l=0}^{2} \Big\{ & J'_{xy}\left(m^x_l m^x_{l+1} + m^y_l m^y_{l+1}\right) + J'_z m^z_l m^z_{l+1} + \sum_{pq}\Big(J'_c\left(\boldsymbol{f}_q\cdot\boldsymbol{n}_s\right)\left(\boldsymbol{f}_q\cdot\boldsymbol{n}_{s'}\right) \\ & + J'_{cz}\left[\left(\boldsymbol{f}_q\cdot\boldsymbol{n}_s\right)n^z_{s'} + n^z_s\left(\boldsymbol{f}_q\cdot\boldsymbol{n}_{s'}\right)\right]\Big)\Big\}, \end{aligned} \tag{26}$$

where

$$\boldsymbol{m}_l = \sum_{p=0}^{2}\boldsymbol{n}_{3l+p} \tag{27}$$

is the total magnetization per unit cell of layer l. Note that in this case the last two terms do not drop out or simplify as they do for the intralayer couplings, because the sublattice indices s and s' are a function of q, which means the q sum is not trivial.

Examining Eq. (26), we see that the XXZ type inter-layer couplings J'_{xy} and J'_z depend on the spin configurations only through the layer magnetizations $\boldsymbol{m}_l$. This *vanishes* in the three-sublattice states favored by the 2d interactions. Thus, at this level, the interlayer XXZ exchanges are completely ineffective at coupling the layers and creating 3d order. This is simply because each spin is symmetrically coupled to three spins on a triangle in the layers above and below it, whose sum is zero. Thus the J'_{xy} and J'_z interactions are fully frustrated by the 2d three-sublattice order.

This conclusion is perturbative in J'_{xy} and J'_z. But in fact the frustration is even stronger. For the XXZ model with $J_c = J'_c = J_{cz} = J'_{cz} = 0$, Rastelli and Tassi[7] have found the exact classical ground states for arbitrary $J_{xy}, J_z, J'_{xy}, J'_z$. In a wide regime, the ground states form a *line of degenerate spirals* which are *close* to the three-sublattice 120° state but have in general an incommensurate wavevector with an *arbitrary*

component k_z normal to the plane. The continuous family of spiral wavevectors echoes the full frustration in the perturbative limit, and shows that frustration remains in the XXZ model non-perturbatively.

We now return to the perturbative analysis, and consider the effects of the anisotropy terms J_c' and J_{cz}'. We suppose each layer has a 120° three-sublattice configuration, and ask how they are coupled. A general form for such a configuration is

$$\hat{\boldsymbol{n}}_{lp} = \begin{pmatrix} \cos(\frac{2\pi\sigma_l p}{3} + \phi_l) \\ \sin(\frac{2\pi\sigma_l p}{3} + \phi_l) \\ 0 \end{pmatrix}, \tag{28}$$

where $\sigma_l = \pm 1$ is the vector spin chirality of the triad of three spins in layer l, and $s = 3l + p$ as usual. For this ansatz, $\boldsymbol{m}_l = 0$. The inter-layer energy becomes

$$\begin{aligned} 9E_{il}/(NS^2) &= J_c' \sum_{l,p,q} \cos\left(\frac{2\pi\sigma_l p}{3} + \phi_l - \frac{\pi}{6} - \frac{2\pi q}{3}\right) \cos\left(\frac{2\pi\sigma_{l+1}(p+q)}{3} + \phi_{l+1} - \frac{\pi}{6} - \frac{2\pi q}{3}\right) \\ &= \frac{J_c'}{2} \sum_{l,p,q} \left[\cos\left(\frac{2\pi(\sigma_l p + \sigma_{l+1}(p+q))}{3} + \phi_l + \phi_{l+1} - \frac{\pi}{3} - \frac{4\pi q}{3}\right) \right. \\ &\qquad \left. + \cos\left(\frac{2\pi(\sigma_l p - \sigma_{l+1}(p+q))}{3} + \phi_l - \phi_{l+1}\right) \right] \\ &= \frac{J_c'}{2} \sum_{l,p,q} \cos\left(\frac{2\pi(\sigma_l p + \sigma_{l+1}(p+q))}{3} + \phi_l + \phi_{l+1} - \frac{\pi}{3} - \frac{4\pi q}{3}\right). \end{aligned} \tag{29}$$

One immediately sees that, because we took an in-plane configuration, J_{cz}' drops out trivially. In passing to the last line we noticed that the sum over q always gives zero in the final term of the previous line, and so dropped it. The final form may also vanish under summation. The sum over q will vanish here unless $\sigma_{l+1} = -1$, in which case the q dependence drops inside the cosine. Then we see that the sum over p will vanish unless $\sigma_l = -\sigma_{l+1} = +1$. So finally we have

$$9E_{il}/(NS^2) = \frac{9}{2} J_c' \sum_l \cos\left(\phi_l + \phi_{l+1} - \frac{\pi}{3}\right) \delta_{\sigma_l,1} \delta_{\sigma_{l+1},-1}. \tag{30}$$

Actually in this analysis we do not need to assume three-fold periodicity in the c direction, and can take l to just sum over all the layers in the crystal.

Based on Eq. (30), we can address how frustrated the remaining J_c' inter-layer coupling is. First, if the chiralities are the same in all layers then the energy due to J_c' vanishes. This is entirely independent of the overall angle ϕ_l within each layer. Second, a pair of adjacent layers can lower its energy by choosing the "lower" one (smaller z) to have "positive" chirality $\sigma_l = 1$ and the upper one negative, and then choosing $\phi_l + \phi_{l+1} = -2\pi/3$ (for $J_c' > 0$). However, the J_c' interaction between the upper layer and the next layer then is guaranteed to vanish, as is the interaction between the lower layer and the next lower one. So the best configuration is one in which layers alternate chirality and gain energy from every other pair. There are two possible staggered orders of chirality. For example, we can take $\sigma_l = (-1)^l$. In this case the energy lowering comes from the interaction between spins with even l and those with odd $l+1$. Moreover, spins in those pairs of layers are correlated, while between these pairs there is no correlation. For $2N$ layers there are N free angles ϕ_{2n} remaining. So there is still quite a bit of degeneracy. However, it is also clear that, in this pattern of spins, translational symmetry by 3 in the vertical direction is necessarily broken.

In summary: the presence of a high degree of degeneracy even once the J_c' interactions have been included indicates that the interlayer coupling of the three-sublattice order is frustrated even with the most general exchange interactions. This suggests a strong suppression of ordering when the 2d exchanges are in this regime, in zero magnetic field (which we have assumed).

2.2.2 Stripe regime

Now we suppose the individual layers are in the stripe regime of the classical phase diagram. We consider the effect of interlayer interactions on these stripes to see how they couple together to form 3d order.

Suppose, as in Eq. (14), the spins in the layer $z = l = 0$ order into ferromagnetic stripes along the x axis, with spins oriented along y. Now consider the next exchange field on the spins in the layer at $z = 1/3$. Each spin in that layer receives contributions from three spins from a triangle in the $z = 0$ layer. Consequently, even for simple Heisenberg or XY coupling J' between the layers, there is a net exchange field on each site in the $z = 1/3$ layer, which aligns those spins into a unique preferred pattern in the next layer. This pattern also consists of ferromagnetic chains along x and moments along y. If one assumes antiferromagnetic J', each spin on the $z = 1/3$ layer is antiparallel to two spins on the triangle below it. Repeating this process leads to a globally determined ordering pattern. The interlayer coupling in the stripe state is therefore *unfrustrated* and the ground state degeneracy of the stripe is just that of a single layer, i.e. 6.

The 3d ordering pattern that results in the way just described has symmetry under a three-dimensional translation by the vector $\boldsymbol{t} = (-\boldsymbol{a}_1 - 2\boldsymbol{a}_2 + \boldsymbol{c})/3$. So due to the in-plane doubled unit cell, in total it has just a doubled unit cell.

The lack of frustration of the interlayer coupling in the stripe state suggests that a system whose 2d interactions favor the stripe order will likely stabilize 3d ordering through the inter-layer interactions. Since this does not occur in $NaYbO_2$, we argue by contradiction that this material is likely to be in the parameter regime in which the 2d exchanges favor three-sublattice 120° order and not the stripe state. This corresponds to the XXZ regime with not too strong J_c interactions.

3 Simulation for the Dynamic Spin Structure Factor

In this Supplemental section, we study the excitations of the 2d triangular XXZ model using linear spin wave theory and present simulation results for the dynamic spin structure factors.

3.1 Linear spin wave theory

Define an orthogonal basis $(\boldsymbol{p}_s, \boldsymbol{q}_s, \boldsymbol{n}_s)$ for each classical spin $\boldsymbol{n}_s$, $s = 0, 1, 2$. The standard Holstein-Primakoff transformation is

$$\boldsymbol{S}_i \cdot \boldsymbol{p}_s = \sqrt{2S}\frac{a_i + a_i^\dagger}{2}, \qquad \boldsymbol{S}_i \cdot \boldsymbol{q}_s = \sqrt{2S}\frac{a_i - a_i^\dagger}{2i}, \qquad \boldsymbol{S}_i \cdot \boldsymbol{n}_s = S - a_i^\dagger a_i, \tag{31}$$

or

$$\boldsymbol{S}_i = \sqrt{2S} M_s K \begin{pmatrix} a_i \\ a_i^\dagger \end{pmatrix} + \boldsymbol{n}_s (S - a_i^\dagger a_i), \tag{32}$$

where $a_i^\dagger$ and a_i are the boson creation and annihilation operators for spin excitations, and we defined

$$M_s = \begin{pmatrix} \boldsymbol{p}_s & \boldsymbol{q}_s \end{pmatrix} \qquad \text{and} \qquad K = \frac{1}{2}\begin{pmatrix} 1 & 1 \\ -i & i \end{pmatrix}. \tag{33}$$

Plugging Eq. (32) into the Hamiltonian (16), keeping terms only of the order S and doing a Fourier transform, we arrive at a quadratic Hamiltonian for the bosons:

$$H_{2d,B}[a, a^\dagger] = \sum_{\boldsymbol{k} \in \mathrm{BZ}^+} \Phi_{\boldsymbol{k}}^\dagger \mathscr{H}(\boldsymbol{k}) \Phi_{\boldsymbol{k}}, \tag{34}$$

where BZ^+ is half of the Brillouin zone which is mapped to the other half by momentum inversion, and we defined $\Phi_{\boldsymbol{k}} = \left(a_{\boldsymbol{k},0}, a_{\boldsymbol{k},1}, a_{\boldsymbol{k},2}, a_{-\boldsymbol{k},0}^\dagger, a_{-\boldsymbol{k},1}^\dagger, a_{-\boldsymbol{k},2}^\dagger\right)^T$,

$$\mathscr{H}(\boldsymbol{k}) = \begin{pmatrix} J_0 & [J_{0,1}]_{11} & [J_{2,0}]_{11}^* & 0 & [J_{0,1}]_{12} & [J_{2,0}]_{21}^* \\ [J_{0,1}]_{11}^* & J_1 & [J_{1,2}]_{11} & [J_{0,1}]_{21}^* & 0 & [J_{1,2}]_{12} \\ [J_{2,0}]_{11} & [J_{1,2}]_{11}^* & J_2 & [J_{2,0}]_{12} & [J_{1,2}]_{21}^* & 0 \\ 0 & [J_{0,1}]_{21} & [J_{2,0}]_{12}^* & J_0 & [J_{0,1}]_{22} & [J_{2,0}]_{22}^* \\ [J_{0,1}]_{12}^* & 0 & [J_{1,2}]_{21} & [J_{0,1}]_{22}^* & J_1 & [J_{1,2}]_{22} \\ [J_{2,0}]_{21} & [J_{1,2}]_{12}^* & 0 & [J_{2,0}]_{22} & [J_{1,2}]_{22}^* & J_2 \end{pmatrix}, \tag{35}$$

and

$$J_{s,s+1} = 2S\left(\sum_{\mu=1,2,3} e^{i\boldsymbol{k}\cdot\boldsymbol{a}_\mu}\right) K^\dagger M_s^\dagger J M_{s+1} K, \tag{36}$$

$$J_s = -3S\boldsymbol{n}_s^T J(\boldsymbol{n}_{s+1}+\boldsymbol{n}_{s-1}) + \mu_B \boldsymbol{B}^T g \boldsymbol{n}_s, \tag{37}$$

where $J \equiv \mathrm{diag}(J_{xy}, J_{xy}, J_z)$, $g = \mathrm{diag}(g_{xy}, g_{xy}, g_z)$. Combined with our knowledge of the classical ground state spin configuration in Sec. 2.1, the following can be deduced:

- The diagonal entries (37) are the classical energy cost of a spin flip $\boldsymbol{S} \to -\boldsymbol{S}$. The flip changes the exchange energy $-3S\boldsymbol{n}_s^T J(\boldsymbol{n}_{s+1}+\boldsymbol{n}_{s-1})$ and the Zeeman energy $\mu_B \boldsymbol{B}^T g \boldsymbol{n}_s$. The off-diagonal entries (36) describe quantum fluctuations due to boson hopping.

- In the easy-plane limit $r > 1$, since all three classical spins have the same z component $n_s^z = \frac{m_z}{r+2}$, we have

  $$J_s = 3SJ_{xy}, \qquad s = 0,1,2. \tag{38}$$

  At $\Gamma = (0,0)$ the spectrum is gapless, due to the Goldstone mode of the broken U(1) symmetry. Furthermore, at $\mathrm{K} = (0, \pm\frac{4\pi}{3\sqrt{3}a})$, the Hamiltonian is purely diagonal, and the energy is just the value of J_s in (38), which is three fold degenerate.

- In the extreme easy-axis limit $r \ll 1$ with a perpendicular field $\boldsymbol{B} = (0,0,1)B$, the system is classical and again we are left with only diagonal elements in the Hamiltonian. The ground state in a large magnetic field range is the up-up-down state with excitation energy

  $$J_0 = J_1 = \mu_B g_z B, \qquad J_2 = 6J_z S - \mu_B g_z B. \tag{39}$$

Finally, let us comment on the criterion of selecting the classical ground state $\boldsymbol{n}_{0,1,2}$ which serves as the input to linear spin wave theory. The issue arises when the classical ground state is degenerate (as in the "canted" phase), and different states in the degeneracy manifold may lead to different dynamic spin structure factor patterns. Whenever degeneracy happens, it can be shown that a classical ground state is fully determined by the choice of in-plane components of the spin vector, $\boldsymbol{m}_s = (n_s^x, n_s^y, 0)$. Without loss of generality we define $|\boldsymbol{m}_0| \le |\boldsymbol{m}_1| \le |\boldsymbol{m}_2|$. Our criterion is always to pick $\boldsymbol{n}_{0,1,2}$ such that $\boldsymbol{m}_0$ and $\boldsymbol{m}_1$ have the smallest angle between them. This criterion is chosen to mimic the fact that, in real triangular systems, quantum fluctuation tends to favor states in the degenerate manifold in which spins are maximally collinear.

3.2 Dynamic spin structure factor

The dynamic spin structure factor, by definition, is

$$\mathscr{S}(\boldsymbol{k},\omega) = \sum_{\mu,\nu}(\delta_{\mu\nu} - (\hat{\boldsymbol{k}})_\mu(\hat{\boldsymbol{k}})_\nu)\sum_{s,s'}\langle m_s^\mu(-\boldsymbol{k},-\omega)\, m_{s'}^\nu(\boldsymbol{k},\omega)\rangle, \tag{40}$$

where $m_s^\mu(\boldsymbol{k},\omega) = \mu_B \sum_\kappa g^{\mu\kappa} S_s^\kappa(\boldsymbol{k},\omega)$, and $\hat{\boldsymbol{k}}$ is the unit vector with orientation of $\boldsymbol{k}$. After some derivation, we can write $S(\boldsymbol{k},\omega)$ concisely as

$$\mathscr{S}(\boldsymbol{k},\omega) = \sum_{e=1,2,3} 2S\mu_B^2 \delta(\omega - \lambda_{\boldsymbol{k}}^e)\left[V^\dagger(\boldsymbol{k})\widetilde{Q}^\dagger \widetilde{M}^\dagger g^\dagger \left(1_{3\times3} - \hat{\boldsymbol{k}}\hat{\boldsymbol{k}}^T\right) g \widetilde{M}\widetilde{Q} V(\boldsymbol{k})\right]_{e,e}, \tag{41}$$

where we defined $\widetilde{M} = \begin{pmatrix} \boldsymbol{p}_0 & \boldsymbol{p}_1 & \boldsymbol{p}_2 & \boldsymbol{q}_0 & \boldsymbol{q}_1 & \boldsymbol{q}_2 \end{pmatrix}$, and $\widetilde{Q} = K \otimes 1_{3\times3}$. V is the matrix that diagonalizes $\mathscr{H}$: $V^\dagger \mathscr{H} V = \Lambda$ with energies stored in the diagonal matrix $\Lambda = \mathrm{diag}(\lambda^1, \lambda^2, \lambda^3, \lambda^1, \lambda^2, \lambda^3)$. Commutation relation of the bosons in the old and the new bases requires $V(\sigma_3 \otimes 1_{3\times3})V^\dagger = \sigma_3 \otimes 1_{3\times3}$.

To connect to the experiment, we define the momentum-orientation-averaged spin structure factor

$$\overline{\mathscr{S}}_{\boldsymbol{B}}(k,\omega) = \frac{1}{4\pi}\int_\pi^0 \sin\theta\, d\theta \int_0^{2\pi} d\phi\, S_{\boldsymbol{B}}(k\sin\theta\cos\phi, k\sin\theta\sin\phi, \omega), \tag{42}$$

where we have used subscript $\boldsymbol{B}$ to remind us of the field dependence. Furthermore, we define the magnetic-orientation-averaged spin structure factor

$$\overline{\overline{\mathscr{S}}}(k,\omega) = \frac{1}{4\pi}\int_{\pi}^{0} \sin\theta_B d\theta_B \int_0^{2\pi} d\phi_B \, \overline{\mathscr{S}}_{B(\sin\theta_B\cos\phi_B,\sin\theta_B,\sin\phi_B,\cos\theta_B)}(k,\omega). \tag{43}$$

Admittedly, such a spin structure factor (43) in which the momentum and magnetic field orientations are *independently* averaged does not fully correspond to the experimental measurement: the neutron scattering measurement averages over the grain orientations of the powder sample, which is equivalent to averaging over momentum and magnetic field orientations that are *locked* with a definite relation. Nevertheless our choice of averaging is justified by the robust spectral features (e.g. the isolated high energy flat intensity) observed in a large region with easy-plane near-Heisenberg exchange and in the extreme easy-axis region.

Now we describe the results for the dynamic spin structure factors. We present two representative parameter points near the Heisenberg limit: the first one has weak easy-axis anisotropy with $(J_z, J_{xy}) = (0.5, 0.45)$ meV, and the second one has weak easy-plane anisotropy with $(J_z, J_{xy}) = (0.45, 0.51)$ meV. The magnetic field is set to be 5 T in both cases but its orientation is varied. The simulated structure factor plots are shown in Fig. 5.

$(J_z, J_{xy}) = (0.5, 0.45)$ meV. When the magnetic field is along z direction, the classical ground state has a coplanar three-sublattice order [see Fig. 5(a)]. The lowest energy band becomes gapless at Γ (Goldstone mode), corresponding to the zero energy structure factor intensity at $|\boldsymbol{Q}| \approx 1.25\text{Å}^{-1}$. The highest energy band is almost flat on the boundary of the magnetic Brilloun zone, which accounts for the structure factor intensity plateau at 0.8 meV. In addition, the highest band has an energy minimum at Γ, which is reflected in the downturn of the high energy intensity plateau at small reciprocal lattice $|\boldsymbol{Q}| \to 0$. As the magnetic field develops an in-plane component [see Fig. 5(b) for $\theta_B = 75°$], the highest band becomes less flat and the highest band energy at Γ increases; at $\theta_B \approx 70°$ Γ becomes the energy maximum, making the structure factor intensity as $|\boldsymbol{Q}| \to 0$ also at the highest energy. The destruction of the high energy flat bands and the appearance of structure factor intensity at the energy maximum as $|\boldsymbol{Q}| \to 0$, both due to large in-plane field component, are generic features of the easy-axis phase region in the parameter range we considered, and consequently one observes an upturn of the high energy intensity as $|\boldsymbol{Q}| \to 0$ in the $\overline{\overline{\mathscr{S}}}(k,\omega)$ plot, with no well-defined isolated high energy intensity plateau.

$(J_z, J_{xy}) = (0.45, 0.51)$ meV. When the magnetic field is along z direction, the classical ground states form a degenerate manifold of the "canted" type. Since the z spin component is small in the parameter range we considered [see Fig. 5(c)], the spin order is almost coplanar, and consequently the spin structure factor resembles the previous case $(J_z, J_{xy}) = (0.5, 0.45)$ meV. In addition to the gapless energy band at Γ (Goldstone mode), three-fold energy degeneracy appears at K and its equivalent points [whose energies are given in Eq. (38)]. There is no global flat energy bands at high energy, and indeed when the magnetic field is along z, there is no well-defined high energy flat intensity in the structure factor plots. Nevertheless, as the magnetic field develops an in-plane component, an *isolated* structure factor intensity plateau emerges as the magnetic field angle θ_B exceeds 30° [see Fig. 5(d)) for $\theta_B = 75°$]. The emergence of such an isolated intensity plateau due to the in-plane field component is a generic feature of the Heisenberg limit with weak easy-plane anisotropy, and persists through $1 < r < 1.6$ in the parameter range we considered. The highest energy band has a local minimum at Γ for all magnetic field orientations (unlike the easy-axis case), which accounts for the downturn of the isolated high energy intensity plateau at small reciprocal lattice $|\boldsymbol{Q}| \to 0$ in the $\overline{\overline{\mathscr{S}}}(k,\omega)$ plot.

4 Supplemental Figures and Tables

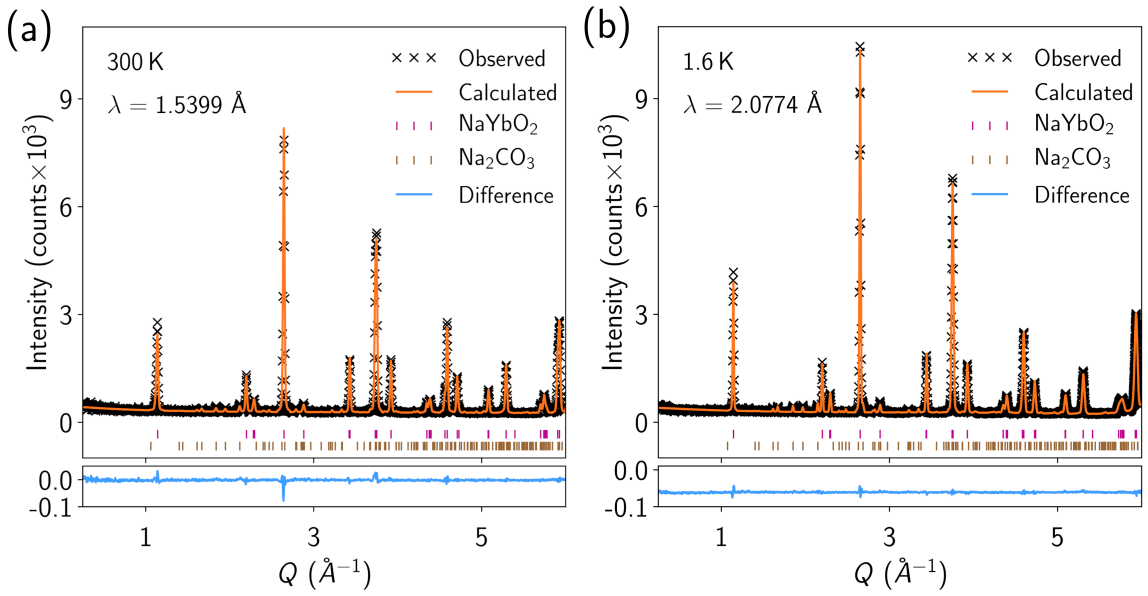

Supplemental Figure 1: Neutron diffraction data collected on $NaYbO_2$. (a) Elastic neutron diffraction pattern collected at 300 K on $NaYbO_2$ powder with λ = 1.5399 Å. (b) Data at 1.6 K were collected with λ = 2.0774 Å and show no new peaks corresponding to a phase transition or magnetic ordering. The weight fraction of Na_2CO_3 refines to 4.1(1)%. Error bars and values in parenthesis represent one standard deviation.

T		300 K					1.6 K				
λ		1.5399 Å					2.0774 Å				
$a = b$		3.35185(3) Å					3.34556(3) Å				
c		16.5319(3) Å					16.4559(3) Å				
Atom	Wyckoff	x	y	z	U_{iso} (Å^2)	Occupancy	x	y	z	U_{iso} (Å^2)	Occupancy
Yb	3a	0	0	0	0.54(2)	1.000(2)	0	0	0	0.53(1)	1.000(2)
Na	3b	0	0	0.5	1.59(7)	0.996(6)	0	0	0.5	0.85(5)	1.000(6)
O	6c	0	0	0.26355(6)	0.83(3)	0.999(3)	0	0	0.26423(6)	0.53(2)	1.000(2)

Supplemental Table 1: Rietveld refinement structural parameters at 300 K and 1.6 K from elastic neutron scattering measurements. Within error, all ions refined to full occupation and did not indicate any mixing between the Na- and Yb-ion sites. Values in parenthesis represent one standard deviation.

	$YbMgGaO_4$ [6]	$NaYbO_2$	
Temperature	300 K $a = b = 3.4037(1)$ Å $c = 25.135(1)$ Å	300 K	1.6 K
Yb-O (Å)	2.2517(1)	2.5301(1)	2.2414(1)
{1} O-Yb-O (deg.)	81.807(1)	83.877(1)	83.459(1)
{2} O-Yb-O (deg.)	98.193(1)	96.123(1)	96.541(1)

Supplemental Table 2: Structural differences in YbO_6 octahedra of $YbMgGaO_4$ (see Paddison et al.[6]) and $NaYbO_2$ at 300 K and 1.6 K from Rietveld refinements of neutron powder diffraction. Both materials share the same $R\bar{3}m$ space group, "ABC" stacking sequence of YbO_6 triangular planes, and local trigonally-compressed D_{3d} YbO_6 octahedra. However, where $YbMgGaO_4$ contains two intermixed Mg/Ga layers between YbO_6 sheets, $NaYbO_2$ contains only one fully-occuped Na layer. Additionally, Yb-Yb ion distances in-plane, equivalent to the a-axis lattice parameter, is shortened in $NaYbO_2$ (Supplemental Table 1). In both materials, there is only one Yb-O distance in the octahedra, but two unique O-Yb-O bond angles. Bond angle {1} refers to the compressed O-Yb-O angle between oxygen layers stacked along the c-axis, while bond angle {2} refers to expanded bond angles within the oxygen layers. At 300 K, $YbMgGaO_4$ displays slightly elongated Yb-O distances with more compressed octahedra than $NaYbO_2$. Also, the trigonal compression of YbO_6 octahedra in $NaYbO_2$ is slightly relieved at 1.6 K. Values in parenthesis represent one standard deviation.

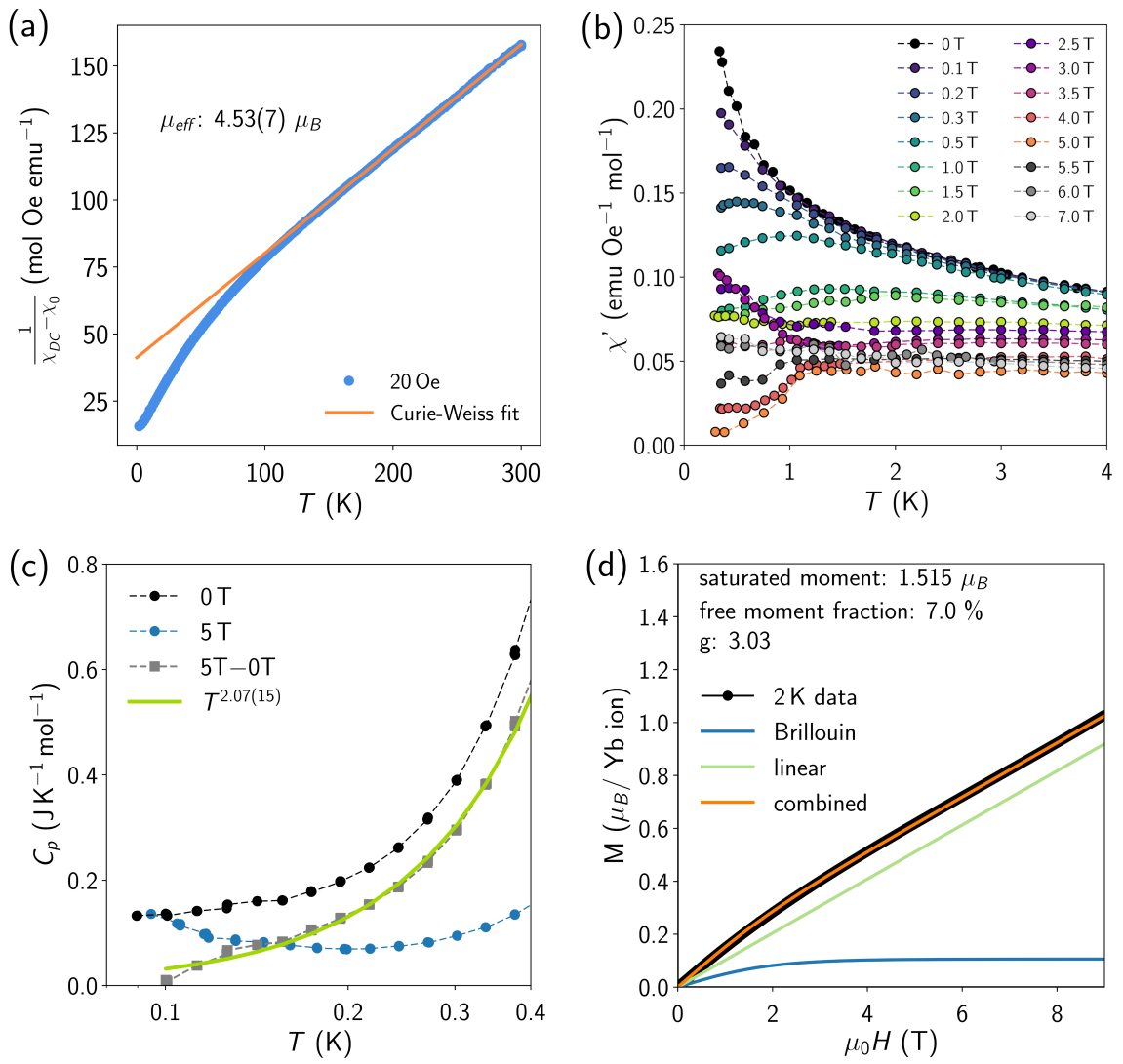

Supplemental Figure 2: Supporting analysis of magnetization, magnetic susceptibility, and heat capacity data. (a) High-temperature susceptibility of $NaYbO_2$ was fit with a Curie-Weiss model between 200K and 300K and produces a linear fit with an average moment close to the free ion value for trivalent Yb ($4.54\mu_B$). However, this temperature regime is influenced by Van Vleck terms from nearby crystal field doublets, meaning that extracted Curie-Weiss temperatures would not accurately represent mean-field interactions between Yb ions. As described in the main text, the low-temperature Curie-Weiss model more accurately captures the interaction strength of Yb ions in the $J_{eff} = 1/2$ state. (b) Combined temperature and field dependence of AC magnetic susceptibility χ'(T) from 300 mK to 4 K showing all collected fields. (c) Specific heat data collected under 0T (black) and 5T (blue) fields that display remnant heat capacity centered around 100 mK likely due to a nuclear Schottky anomaly. A cross check of the power law fit of data in the 0T quantum-disordered phase (green) was obtained by subtracting out the field-independent Schottky anomaly using 5T data (grey) in the antiferromagnetically ordered state where low energy spin fluctuations are suppressed. The fit value obtained between 100 − 400mK is in agreement with that in the main text. (d) Magnetization data collected at 2 K. Data show the response up to 9 T fit to a two-component model. The low field data was fit to a Brillouin fit assuming the average g-factor and $J_{eff} = 1/2$ moments with a variable volume fraction, and the high field part was fit to a linear response due to the strong antiferromagentic exchange field. The fraction of free spins determined from this model is ≈ 7%, in rough agreement with the Curie-Weiss analysis presented in the main text. Error bars and values in parenthesis represent one standard deviation.

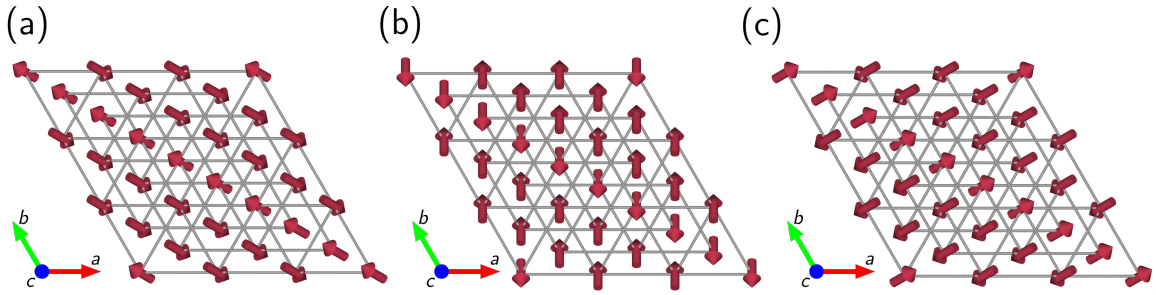

Supplemental Figure 3: Top-down views of magnetic unit cells refined from field subtracted powder neutron diffraction data at 450 mK (5 T−0 T) as described in the main text (Fig 4). Due to the three-fold symmetry of the structure, three symmetry equivalent **q**-vectors can describe the neutron diffraction data with corresponding basis vectors and spin structures. All structures consist of collinear Yb moments. (a) As shown in the main text Fig. 4, the ordering wave vector of **q**=$(1/3, 1/3, 0)$ creates a magnetic state of Yb spins approximately along the $< 1, -1, -1 >$ direction. (b) The wave vector of **q**=$(2/3, -1/3, 0)$ contains moments aligned near the $< 1, 2, -1 >$ direction. (c) With an ordering wave vector of **q**=$(1/3, -2/3, 0)$, moments align close to the $< -2, -1, -1 >$ direction.

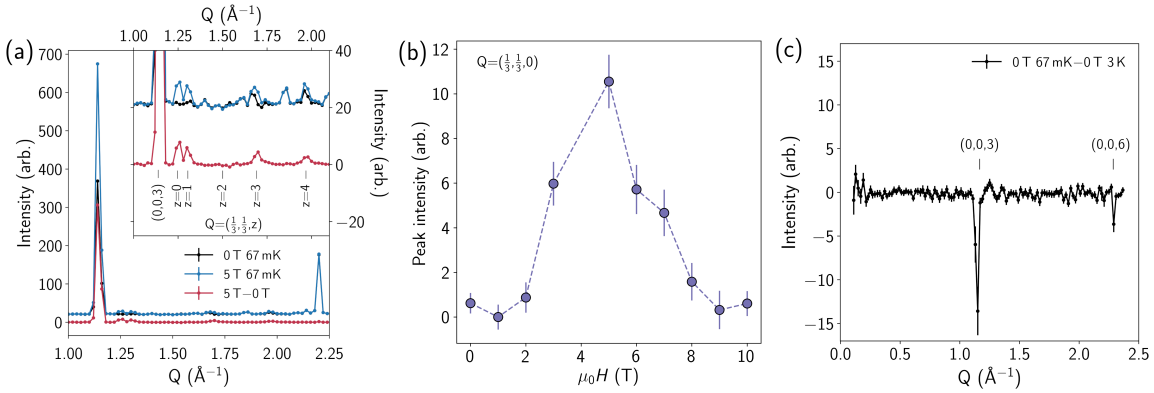

Supplemental Figure 4: Neutron powder diffraction data collected on the DCS instrument at the NIST Center for Neutron Research. (a) 67 mK elastic scattering data integrated from -0.1 meV to 0.1 meV plotted as a function of momentum transfer under both zero field and 5T. Subtracted 5T - 0T data are also plotted and the inset shows a zoomed in region where the (1/3, 1/3, L)-type antiferromagnetic peaks appear under field. (b) Field dependence of the (1/3, 1/3, 0) magnetic Bragg peak. The integrated intensity of the peak is plotted versus the applied magnetic field. (c) Zero field diffraction data showing the subtraction of 67 mK and 3 K data and the absence of zero field magnetic order. The oversubtraction of intensities at the nuclear Bragg positions (0,0,3) and (0,0,6) is due to slight alignment/polarization of the loose powder upon cycling field between the 67 mK and 3 K measurements. Error bars represent one standard deviation.

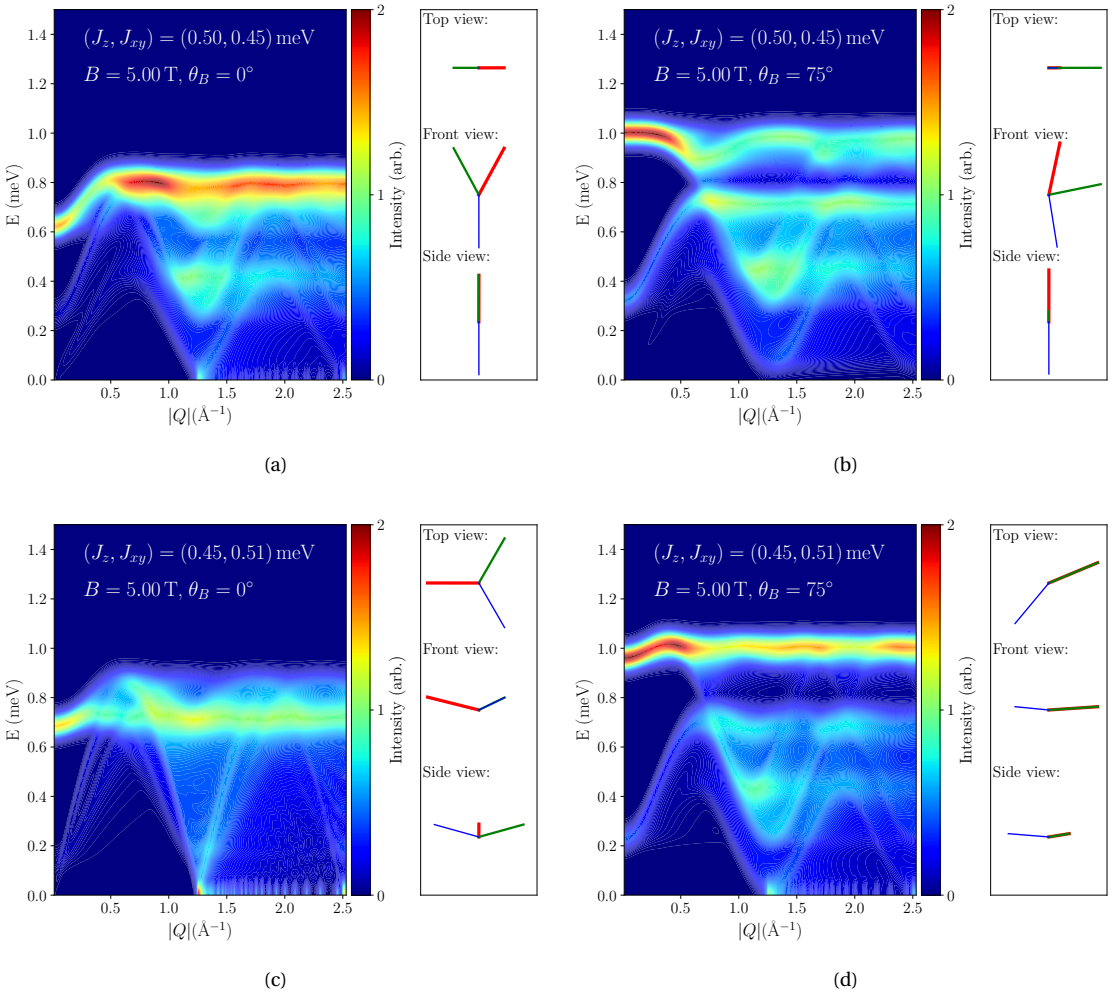

Supplemental Figure 5: Dynamic spin structure factor $\overline{\mathscr{S}}(k,\omega)$ and the classical three-sublattice (red, green and blue) spin ground state from different views. The exchange parameters are (a,b) $(J_z, J_{xy}) = (0.5, 0.45)$ meV, and (c,d) $(J_z, J_{xy}) = (0.45, 0.51)$ meV. Field strength is fixed at $B = 5$ T, while the field orientation is tilted from the z axis with an angle of either (a,c) $\theta_B = 0°$ or (b,d) $\theta_B = 75°$.

References

[1] Jason Iaconis, Chunxiao Liu, Gábor Halász, and Leon Balents. Spin liquid versus spin orbit coupling on the triangular lattice. *SciPost Physics*, 4(1):003, 2018.

[2] Yao-Dong Li, Xiaoqun Wang, and Gang Chen. Anisotropic spin model of strong spin-orbit-coupled triangular antiferromagnets. *Physical Review B*, 94(3):035107, 2016.

[3] Yuesheng Li, Gang Chen, Wei Tong, Li Pi, Juanjuan Liu, Zhaorong Yang, Xiaoqun Wang, and Qingming Zhang. Rare-earth triangular lattice spin liquid: A single-crystal study of $ybmggao_4$. *Phys. Rev. Lett.*, 115:167203, Oct 2015.

[4] Qiang Luo, Shijie Hu, Bin Xi, Jize Zhao, and Xiaoqun Wang. Ground-state phase diagram of an anisotropic spin-1 2 model on the triangular lattice. *Physical Review B*, 95(16):165110, 2017.

[5] Zohar Nussinov and Jeroen Van Den Brink. Compass models: Theory and physical motivations. *Reviews of Modern Physics*, 87(1):1, 2015.

[6] Joseph A.M. Paddison, Marcus Daum, Zhiling Dun, Georg Ehlers, Yaohua Liu, Matthew B. Stone, Haidong Zhou, and Martin Mourigal. Continuous excitations of the triangular-lattice quantum spin liquid $ybmggao_4$. *Nature Physics*, 13:117, Dec 2017.

[7] E Rastelli and A Tassi. The rhombohedral heisenberg antiferromagnet: infinite degeneracy of the ground state and magnetic properties of solid oxygen. *Journal of Physics C: Solid State Physics*, 19(19):L423, 1986.

[8] Daisuke Yamamoto, Giacomo Marmorini, and Ippei Danshita. Quantum phase diagram of the triangular-lattice xxz model in a magnetic field. *Phys. Rev. Lett.*, 112:127203, Mar 2014.

[9] Zhenyue Zhu, P. A. Maksimov, Steven R. White, and A. L. Chernyshev. Topography of spin liquids on a triangular lattice. *Phys. Rev. Lett.*, 120:207203, May 2018.